

# Equation of state, universal profiles, scaling and macroscopic quantum effects in Warm Dark Matter galaxies

H. J. de Vega <sup>(a,b)\*</sup> and N. G. Sanchez <sup>(b)†</sup>

<sup>(a)</sup> *LPTHE, Université Pierre et Marie Curie (Paris VI),  
Laboratoire Associé au CNRS UMR 7589, Tour 24, 5ème. étage,  
Boite 126, 4, Place Jussieu, 75252 Paris, Cedex 05, France.*

<sup>(b)</sup> *Observatoire de Paris, LERMA. Laboratoire Associé au CNRS UMR 8112,  
61, Avenue de l'Observatoire, 75014 Paris, France.*

(Dated: June 23, 2021)

The Thomas-Fermi approach to galaxy structure determines selfconsistently and non-linearly the gravitational potential of the fermionic warm dark matter (WDM) particles given their quantum distribution function  $f(E)$ . This semiclassical framework accounts for the quantum nature and high number of DM particles, properly describing gravitational bounded and quantum macroscopic systems as neutron stars, white dwarfs and WDM galaxies. We express the main galaxy magnitudes as the halo radius  $r_h$ , mass  $M_h$ , velocity dispersion and phase space density in terms of the surface density which is important to confront to observations. From these expressions we **derive** the general equation of state for galaxies, i. e., the relation between pressure and density, and provide its analytic expression. Two regimes clearly show up: (i) Large diluted galaxies for  $M_h \gtrsim 2.3 \cdot 10^6 M_\odot$  and effective temperatures  $T_0 > 0.017$  K described by the classical selfgravitating WDM Boltzman gas with an inhomogeneous perfect gas equation of state, and (ii) Compact dwarf galaxies for  $1.6 \cdot 10^6 M_\odot \gtrsim M_h \gtrsim M_{h,min} \simeq 3.10 \cdot 10^4 (2 \text{ keV}/m)^{\frac{16}{5}} M_\odot$ ,  $T_0 < 0.011$  K described by the quantum fermionic WDM regime with a steeper equation of state close to the degenerate state. In particular, the  $T_0 = 0$  degenerate or extreme quantum limit yields the most compact and smallest galaxy. All magnitudes in the diluted regime turn to exhibit square root of  $M_h$  **scaling** laws and are **universal** functions of  $r/r_h$  reflecting the WDM perfect gas behaviour in this regime. These theoretical results contrasted to robust and independent sets of galaxy data remarkably reproduce the observations. For the small galaxies,  $10^6 \gtrsim M_h \geq M_{h,min}$ , the equation of state is galaxy mass dependent and the density and velocity profiles are not anymore universal, accounting to the quantum physics of the self-gravitating WDM fermions in the compact regime (near, but not at, the degenerate state). It would be extremely interesting to dispose of dwarf galaxy observations which could check these quantum effects.

## Contents

<b>I. INTRODUCTION</b>	1
<b>II. Galaxy structure in the WDM Thomas-Fermi approach</b>	4
A. Galaxy properties in the diluted Boltzmann regime	9
<b>III. Density and velocity dispersion. Universal and non-universal profiles</b>	14
<b>IV. The equation of state of WDM Galaxies. Classical diluted and compact quantum regimes.</b>	16
<b>V. The dependence on the WDM particle mass in the diluted and quantum regimes</b>	20
<b>References</b>	20

## I. INTRODUCTION

Dark matter (DM) is the main component of galaxies: the fraction of DM over the total galaxy mass goes from 95% for large diluted galaxies till 99.99% for dwarf compact galaxies. Therefore, DM alone should explain the main

---

\*Electronic address: devega@lpthe.jussieu.fr

†Electronic address: Norma.Sanchez@obspm.fr

structure of galaxies. Baryons should only give corrections to the pure DM results.

Warm Dark Matter (WDM), that is dark matter formed by particles with masses in the keV scale receives increasing attention today ([6, 16, 17] and references therein).

At intermediate scales  $\sim 100$  kpc, WDM gives the **correct abundance** of substructures and therefore WDM solves the cold dark matter (CDM) overabundance of structures at small scales. [1, 4, 15, 20, 21, 27, 33, 35, 38]. For scales larger than 100 kpc, WDM yields the same results than CDM. Hence, WDM agrees with all the observations: small scale as well as large scale structure observations and CMB anisotropy observations.

Astronomical observations show that the DM galaxy density profiles are **cored** till scales below the kpc [29, 30, 39]. On the other hand,  $N$ -body CDM simulations exhibit cusped density profiles with a typical  $1/r$  behaviour near the galaxy center  $r = 0$ . Inside galaxy cores, below  $\sim 100$  pc,  $N$ -body classical physics simulations do not provide the correct structures for WDM because quantum effects are important in WDM at these scales. Classical physics  $N$ -body WDM simulations exhibit cusps or small cores with sizes smaller than the observed cores [2, 5, 22, 36]. WDM predicts correct structures and cores with the right sizes for small scales (below kpc) when the **quantum** nature of the WDM particles is taken into account [7, 8]. This approach is **independent** of any WDM particle physics model.

We follow here the Thomas-Fermi approach to galaxy structure for self-gravitating fermionic WDM [7, 8]. This approach is especially appropriate to take into account quantum properties of systems with large number of particles. That is, macroscopic quantum systems as neutron stars and white dwarfs [19]. In this approach, the central quantity to derive is the DM chemical potential  $\mu(\mathbf{r})$ , which is the free energy per particle. For self-gravitating systems, the potential  $\mu(\mathbf{r})$  is proportional to the gravitational potential  $\phi(\mathbf{r})$ ,  $\mu(\mathbf{r}) = \mu_0 - m \phi(\mathbf{r})$ ,  $\mu_0$  being a constant, and obeys the **self-consistent** and **nonlinear** Poisson equation

$$\nabla^2 \mu(\mathbf{r}) = -4 \pi g G m^2 \int \frac{d^3 p}{(2 \pi \hbar)^3} f \left( \frac{p^2}{2m} - \mu(\mathbf{r}) \right). \quad (1.1)$$

Here  $G$  is Newton's gravitational constant,  $g$  is the number of internal degrees of freedom of the DM particle,  $p$  is the DM particle momentum and  $f(E)$  is the energy distribution function. This is a semiclassical gravitational approach to determine selfconsistently the gravitational potential of the quantum fermionic WDM given its distribution function  $f(E)$ .

In the Thomas-Fermi approach, DM dominated galaxies are considered in a stationary state. This is a realistic situation for the late stages of structure formation since the free-fall (Jeans) time  $t_{ff}$  for galaxies is much shorter than the age of galaxies.  $t_{ff}$  is at least one or two orders of magnitude smaller than the age of the galaxy.

We consider spherical symmetric configurations where eq.(1.1) becomes an ordinary nonlinear differential equation that determines self-consistently the chemical potential  $\mu(r)$  and constitutes the Thomas-Fermi approach [7, 8]. We choose for the energy distribution function a Fermi-Dirac distribution

$$f(E) = \frac{1}{e^{E/T_0} + 1},$$

where  $T_0$  is the characteristic one-particle energy scale.  $T_0$  plays the role of an effective temperature scale and depends on the galaxy mass. The Fermi-Dirac distribution function is justified in the inner regions of the galaxy, inside the halo radius where we find that the Thomas-Fermi density profiles perfectly agree with the observations.

The solutions of the Thomas-Fermi equations (1.1) are characterized by the value of the chemical potential at the origin  $\mu(0)$ . Large positive values of  $\mu(0)$  correspond to dwarf compact galaxies (fermions near the quantum degenerate limit), while large negative values of  $\mu(0)$  yield large and diluted galaxies (classical Boltzmann regime).

Approaching the classical diluted limit yields larger and larger halo radii, galaxy masses and velocity dispersions. On the contrary, in the quantum degenerate limit we get solutions of the Thomas-Fermi equations corresponding to the **minimal** halo radii, galaxy masses and velocity dispersions.

The surface density

$$\Sigma_0 \equiv r_h \rho_0 \simeq 120 M_\odot/\text{pc}^2 \quad \text{up to } 10\% - 20\%, \quad (1.2)$$

has the remarkable property of being nearly **constant** and independent of luminosity in different galactic systems (spirals, dwarf irregular and spheroidals, elliptics) spanning over 14 magnitudes in luminosity and over different Hubble types [14, 34]. It is therefore a useful characteristic scale to express galaxy magnitudes.

Our theoretical results follow by solving the self-consistent and nonlinear Poisson equation eq.(1.1) which is **solely** derived from the purely **gravitational** interaction of the WDM particles and their **fermionic** nature.

The main galaxy magnitudes as the halo radius  $r_h$ , mass  $M_h$ , velocity dispersion and phase space density are analytically obtained and expressed in terms of the surface density, which is particularly appropriated to confront to observations over the whole range of galaxies.

In this paper we **derive** and analyze the general equation of state of galaxies which clearly exhibits two regimes: (i) Large diluted galaxies for  $M_h \gtrsim 3.7 \cdot 10^6 M_\odot$ ,  $\nu_0 \equiv [\mu(0)/T_0] < -5$ ,  $T_0 > 0.017$  K, described by the classical WDM Boltzmann regime and (ii) Compact dwarf galaxies for  $1.6 \cdot 10^6 \lesssim M_h \geq M_{h,min} \simeq 3.10 \cdot 10^4 (2 \text{ keV}/m)^{\frac{16}{5}} M_\odot$ ,  $\nu_0 > -4$ ,  $T_0 < 0.011$  K described by the quantum fermionic regime close to the degenerate state.

In particular, the  $T_0 = 0$  degenerate or extreme quantum limit yields the most compact and smallest galaxy: with minimal mass  $M_{h,min}$  and minimal radius, and maximal phase space density.

We find that all magnitudes in the diluted regime exhibit square root of  $M_h$  **scaling** laws and are **universal** functions of  $r/r_h$  normalized to their values at the origin or at  $r_h$ . Conversely, the halo mass  $M_h$  scales as the square of the halo radius  $r_h$  as

$$M_h = 1.75572 \Sigma_0 r_h^2 \quad .$$

Moreover, the proportionality factor in this scaling relation is confirmed by the galaxy data (see fig. 2).

We find that the universal theoretical density profile obtained from the Thomas–Fermi equation (1.1) in the diluted regime ( $M_h \gtrsim 10^6 M_\odot$ ) is accurately reproduced by the simple formula (see fig. 5)

$$\frac{\rho(r)}{\rho(0)} = \frac{1}{\left[1 + \left(4^{\frac{1}{\alpha}} - 1\right) \left(\frac{r}{r_h}\right)^2\right]^\alpha} \quad , \quad \alpha = 1.5913 \quad .$$

The fit being precise for  $r < 2 r_h$ .

The theoretical rotation curves and density profiles obtained from the Thomas-Fermi equations remarkably agree with observations for  $r \lesssim r_h$ , for all galaxies in the diluted regime [13]. This indicates that WDM is thermalized in the internal regions  $r \lesssim r_h$  of galaxies.

We find the WDM galaxy equation of state, that is, the functional relation between the pressure  $P$  and the density  $\rho$  in a parametric way as

$$\rho = \frac{m^{\frac{5}{2}}}{3 \pi^2 \hbar^3} (2 T_0)^{\frac{3}{2}} I_2(\nu) \quad , \quad P = \frac{m^{\frac{3}{2}}}{15 \pi^2 \hbar^3} (2 T_0)^{\frac{5}{2}} I_4(\nu) \quad . \quad (1.3)$$

These equations express parametrically, through the parameter  $\nu$ , the pressure  $P$  as a function of the density  $\rho$  and therefore provide the equation of state.  $I_2(\nu)$  and  $I_4(\nu)$  are integrals (2nd and 4th momenta) of the distribution function. At thermal equilibrium they are given by eq.(2.15). For the main galaxy physical magnitudes, the Fermi–Dirac distribution gives similar results than the out of equilibrium distribution functions [8]. We plot in figs. 7 and 8,  $P$  as a function of  $\rho$  for different values of the effective temperature  $T_0$ .

Interestingly enough, we provide a simple formula representing the exact equation of state (1.3) obtained by solving the Thomas-Fermi equation (1.1)

$$P = \frac{m^{\frac{3}{2}} (2 T_0)^{\frac{5}{2}}}{15 \pi^2 \hbar^3} \left(1 + \frac{3}{2} e^{-\beta_1 \tilde{\rho}}\right) \tilde{\rho} \frac{1}{3} (5 - 2 e^{-\beta_2 \tilde{\rho}}) \quad , \quad (1.4)$$

where

$$\tilde{\rho} \equiv \frac{3 \pi^2 \hbar^3}{m^{\frac{5}{2}} (2 T_0)^{\frac{3}{2}}} \rho = I_2(\nu) \quad , \quad (1.5)$$

and the best fit to the exact values of  $P$  as a function  $\tilde{\rho}$  is obtained for the values of the parameters:

$$\beta_1 = 0.047098 \quad , \quad \beta_2 = 0.064492 \quad . \quad (1.6)$$

The fitting formula eq.(1.4) exactly fulfils the diluted and degenerate limiting behaviours:

$$P = \frac{T_0}{m} \rho \quad \text{WDM diluted galaxies} \quad , \quad P = \frac{\hbar^2}{5} \left(\frac{3 \pi^2}{m^4}\right)^{\frac{2}{3}} \rho^{\frac{5}{3}} \quad \text{WDM degenerate quantum limit} \quad .$$

We plot in fig. 9 the exact equation of state obtained by solving the Thomas-Fermi equation and the empirical equation of state eq.(1.4).

We find that the presence of universal profiles in galaxies reflect the perfect gas behaviour of the the WDM galaxy equation of state in the diluted regime which is identical to the self-gravitating Boltzman WDM gas.

These theoretical results contrasted to robust and independent sets of galaxy data remarkably reproduce the observations.

For the small galaxies,  $10^6 M_\odot \gtrsim M_h \geq M_{h,min}$  corresponding to effective temperatures  $T_0 \lesssim 0.017$  K, the equation of state is steeper, dependent on the galaxy mass and the profiles are not anymore universal. These non-universal properties in small galaxies account to the quantum physics of the self-gravitating WDM fermions in the compact regime with high density close to, but not at, the degenerate state.

It would be extremely interesting to dispose of observations which could check these quantum effects in dwarf galaxies.

In summary, the results of this paper show the power and cleanliness of the Thomas-Fermi theory and WDM to properly describe the galaxy structures and the galaxy physical states.

This paper is organized as follows. In Section 2 we present the Thomas-Fermi approach to galaxy structure, we express the main galaxy magnitudes in terms of the solution of the Thomas-Fermi equation and the value of the surface density  $\Sigma_0$ . We analyze the diluted classical galaxy magnitudes, derive their scaling laws and find the universal density and velocity profiles and their agreement with observations.

In Section 3 we derive the equation of state of galaxies and analyze their main regimes: classical regime which is the perfect inhomogenous equation of state, identical to the WDM selfgravitating gas equation of state, and the quantum regime, which exhibits a steeper equation of state, non universal, galaxy mass dependent and describes the quantum fermionic compact states (dwarf galaxies), close to the degenerate limit. Finally, the invariance and dependence on the WDM particle mass  $m$  in the classical and quantum regimes is discussed.

## II. GALAXY STRUCTURE IN THE WDM THOMAS-FERMI APPROACH

We consider DM dominated galaxies in their late stages of structure formation when they are relaxing to a stationary situation, at least not too far from the galaxy center.

This is a realistic situation since the free-fall (Jeans) time  $t_{ff}$  for galaxies is much shorter than the age of galaxies:

$$t_{ff} = \frac{1}{\sqrt{G \rho_0}} = 1.49 \cdot 10^7 \sqrt{\frac{M_\odot}{\rho_0 \text{ pc}^3}} \text{ yr} .$$

The observed central densities of galaxies yield free-fall times in the range from 15 million years for ultracompact galaxies till 330 million years for large diluted spiral galaxies. These free-fall (or collapse) times are small compared with the age of galaxies running in billions of years.

Hence, we can consider the DM described by a time independent and non-relativistic energy distribution function  $f(E)$ , where  $E = p^2/(2m) - \mu$  is the single-particle energy,  $m$  is the mass of the DM particle and  $\mu$  is the chemical potential [7, 8] related to the gravitational potential  $\phi(\mathbf{r})$  by

$$\mu(\mathbf{r}) = \mu_0 - m \phi(\mathbf{r}) , \quad (2.1)$$

where  $\mu_0$  is a constant.

In the Thomas-Fermi approach,  $\rho(\mathbf{r})$  is expressed as a function of  $\mu(\mathbf{r})$  through the standard integral of the DM phase-space distribution function over the momentum

$$\rho(\mathbf{r}) = \frac{g m}{2 \pi^2 \hbar^3} \int_0^\infty dp p^2 f \left[ \frac{p^2}{2m} - \mu(\mathbf{r}) \right] , \quad (2.2)$$

where  $g$  is the number of internal degrees of freedom of the DM particle, with  $g = 1$  for Majorana fermions and  $g = 2$  for Dirac fermions.

We will consider spherical symmetric configurations. Then, the Poisson equation for  $\phi(r)$  takes the self-consistent form

$$\frac{d^2 \mu}{dr^2} + \frac{2}{r} \frac{d\mu}{dr} = -4\pi G m \rho(r) = -\frac{2 g G m^2}{\pi \hbar^3} \int_0^\infty dp p^2 f \left[ \frac{p^2}{2m} - \mu(r) \right] , \quad (2.3)$$

where  $G$  is Newton's constant and  $\rho(r)$  is the DM mass density.

Eq. (2.3) provides an ordinary **nonlinear** differential equation that determines **self-consistently** the chemical potential  $\mu(r)$  and constitutes the Thomas–Fermi approach [7, 8] (see also ref. [9]). This is a semi-classical approach to galaxy structure in which the quantum nature of the DM particles is taken into account through the quantum statistical distribution function  $f(E)$ .

The DM pressure and the velocity dispersion can also be expressed as integrals over the DM phase–space distribution function as

$$P(r) = \frac{g}{6\pi^2 m \hbar^3} \int_0^\infty dp p^4 f \left[ \frac{p^2}{2m} - \mu(r) \right], \quad (2.4)$$

$$\langle v^2 \rangle (r) = \frac{1}{m^2} \frac{\int_0^\infty dp p^4 f \left[ \frac{p^2}{2m} - \mu(r) \right]}{\int_0^\infty dp p^2 f \left[ \frac{p^2}{2m} - \mu(r) \right]}. \quad (2.5)$$

Eqs.(2.2), (2.4) and (2.5) imply the equation of state

$$P(r) = \frac{1}{3} \langle v^2 \rangle (r) \rho(r) = \sigma^2(r) \rho(r). \quad (2.6)$$

It must be stressed that the Thomas–Fermi equation (2.3) determine  $\sigma^2(r)$  in terms of  $\rho(r)$  through eq.(2.5). Therefore, the Thomas–Fermi equation **determines the equation of state** through eq.(2.6). Contrary to the usual situation [3], we **do not assume** the equation of state, but we **derive** it from the Thomas–Fermi equation.

The fermionic DM mass density  $\rho$  is bounded at the origin due to the Pauli principle [7] which implies the bounded boundary condition at the origin

$$\frac{d\mu}{dr}(0) = 0. \quad (2.7)$$

We see that  $\mu(r)$  fully characterizes the DM halo structure in this Thomas–Fermi framework. The chemical potential is monotonically decreasing in  $r$  since eq.(2.3) implies

$$\frac{d\mu}{dr} = -\frac{G m M(r)}{r^2}, \quad M(r) = 4\pi \int_0^r dr' r'^2 \rho(r'). \quad (2.8)$$

From eq.(2.4) and (2.5) we derive the hydrostatic equilibrium equation

$$\frac{dP}{dr} + \rho(r) \frac{d\phi}{dr} = 0. \quad (2.9)$$

Eliminating  $P(r)$  between eqs.(2.6) and (2.9) and integrating on  $r$  gives

$$\frac{\rho(r)}{\rho(0)} = \frac{\sigma^2(0)}{\sigma^2(r)} e^{-\int_0^r \frac{dr'}{\sigma^2(r')} \frac{d\phi}{dr'}}. \quad (2.10)$$

Inserting this expression in the Poisson's equation yields

$$\frac{d^2\phi}{dr^2} + \frac{2}{r} \frac{d\phi}{dr} = 4\pi G \rho_0 \frac{\sigma^2(0)}{\sigma^2(r)} e^{-\int_0^r \frac{dr'}{\sigma^2(r')} \frac{d\phi}{dr'}}. \quad (2.11)$$

This nonlinear equation for non constant  $\sigma^2(r)$  generalizes the corresponding equation in the self-gravitating Boltzmann gas. For constant  $\sigma^2(r)$  eq.(2.10) reduces to the baryotropic equation.

In this semi-classical framework the stationary energy distribution function  $f(E)$  must be given. We consider the Fermi–Dirac distribution

$$f(E) = \Psi_{\text{FD}}(E/T_0) = \frac{1}{e^{E/T_0} + 1}, \quad (2.12)$$

where the characteristic one-particle energy scale  $T_0$  in the DM halo plays the role of an effective temperature. The value of  $T_0$  depends on the galaxy mass. In neutron stars, where the neutron mass is about six orders of magnitude larger than the WDM particle mass, the temperature can be approximated by zero. In galaxies,  $T_0 \sim m \langle v^2 \rangle$  turns to be non-zero but small in the range:  $10^{-3} \text{ K} \lesssim T_0 \lesssim 10 \text{ K}$  for halo galaxy masses in the range  $10^5 - 10^{12} M_\odot$  which reproduce the observed velocity dispersions for  $m \simeq 2 \text{ keV}$ . The smaller values of  $T_0$  correspond to compact dwarfs and the larger values of  $T_0$  are for large and diluted galaxies.

Notice that for the relevant galaxy physical magnitudes, the Fermi-Dirac distribution give similar results than the out of equilibrium distribution functions [8].

The choice of  $\Psi_{\text{FD}}$  is justified in the inner regions, where relaxation to thermal equilibrium is possible. Far from the origin however, the Fermi-Dirac distribution as its classical counterpart, the isothermal sphere, produces a mass density tail  $1/r^2$  that overestimates the observed tails of the galaxy mass densities. Indeed, the classical regime  $\mu/T_0 \rightarrow -\infty$  is attained for large distances  $r$  since eq.(2.8) indicates that  $\mu(r)$  is always monotonically decreasing with  $r$ .

More precisely, large positive values of the chemical potential at the origin correspond to the degenerate fermions limit which is the extreme quantum case and oppositely, large negative values of the chemical potential at the origin gives the diluted case which is the classical regime. The quantum degenerate regime describes dwarf and compact galaxies while the classical and diluted regime describes large and diluted galaxies. In the classical regime, the Thomas-Fermi equation (2.3)-(2.7) become the equations for a self-gravitating Boltzmann gas.

It is useful to introduce dimensionless variables  $\xi$ ,  $\nu(\xi)$

$$r = l_0 \xi \quad , \quad \mu(r) = T_0 \nu(\xi) \quad , \quad f(E) = \Psi(E/T_0) \quad , \quad (2.13)$$

where  $l_0$  is the characteristic length that emerges from the dynamical equation (2.3):

$$l_0 \equiv \frac{\hbar}{\sqrt{8G}} \left(\frac{2}{g}\right)^{\frac{1}{3}} \left[\frac{9\pi I_2(\nu_0)}{m^8 \rho_0}\right]^{\frac{1}{6}} = R_0 \left(\frac{2 \text{ keV}}{m}\right)^{\frac{4}{3}} \left(\frac{2}{g}\right)^{\frac{1}{3}} \left[\frac{I_2(\nu_0)}{\rho_0} \frac{M_\odot}{\text{pc}^3}\right]^{\frac{1}{6}} \quad , \quad R_0 = 7.425 \text{ pc} \quad , \quad (2.14)$$

and

$$I_n(\nu) \equiv (n+1) \int_0^\infty y^n dy \Psi_{FD}(y^2 - \nu) \quad , \quad n = 1, 2, \dots \quad , \quad \nu_0 \equiv \nu(0) \quad , \quad \rho_0 = \rho(0) \quad , \quad (2.15)$$

where we use the integration variable  $y \equiv p/\sqrt{2mT_0}$ . For definiteness, we will take  $g = 2$ , Dirac fermions in the sequel. One can easily translate from Dirac to Majorana fermions changing the WDM fermion mass as:

$$m \Rightarrow \frac{m}{2^{\frac{1}{4}}} = 0.8409 m \quad .$$

Then, in dimensionless variables, the self-consistent Thomas-Fermi equation (2.3) for the chemical potential  $\nu(\xi)$  takes the form

$$\frac{d^2\nu}{d\xi^2} + \frac{2}{\xi} \frac{d\nu}{d\xi} = -I_2(\nu) \quad , \quad \nu'(0) = 0 \quad . \quad (2.16)$$

We find the main physical galaxy magnitudes, such as the mass density  $\rho(r)$ , the velocity dispersion  $\sigma^2(r) = v^2(r)/3$  and the pressure  $P(r)$ , which are all  $r$ -dependent as:

$$\rho(r) = \frac{m^{\frac{5}{2}}}{3\pi^2 \hbar^3} (2T_0)^{\frac{3}{2}} I_2(\nu(\xi)) = \rho_0 \frac{I_2(\nu(\xi))}{I_2(\nu_0)} \quad , \quad \rho_0 = \frac{m^{\frac{5}{2}}}{3\pi^2 \hbar^3} (2T_0)^{\frac{3}{2}} I_2(\nu_0) \quad , \quad (2.17)$$

$$P(r) = \frac{m^{\frac{3}{2}}}{15\pi^2 \hbar^3} (2T_0)^{\frac{5}{2}} I_4(\nu(\xi)) = \frac{1}{5} (9\pi^4)^{\frac{1}{3}} \left(\frac{\hbar^6}{m^8}\right)^{\frac{1}{3}} \left[\frac{\rho_0}{I_2(\nu_0)}\right]^{5/3} I_4(\nu(\xi)) \quad , \quad (2.18)$$

$$\sigma^2(r) = \frac{P(r)}{\rho(r)} = \frac{2T_0}{5m} \frac{I_4(\nu(\xi))}{I_2(\nu(\xi))} \quad . \quad (2.19)$$

As a consequence, from eqs.(2.8), (2.13), (2.14), (2.17) and (2.19) the total mass  $M(r)$  enclosed in a sphere of radius  $r$  and the phase space density  $Q(r)$  turn to be

$$M(r) = 4 \pi \frac{\rho_0 l_0^3}{I_2(\nu_0)} \int_0^\xi dx x^2 I_2(\nu(x)) = 4 \pi \frac{\rho_0 l_0^3}{I_2(\nu_0)} \xi^2 |\nu'(\xi)| = \quad (2.20)$$

$$= M_0 \xi^2 |\nu'(\xi)| \left( \frac{\text{keV}}{m} \right)^4 \sqrt{\frac{\rho_0}{I_2(\nu_0)} \frac{\text{pc}^3}{M_\odot}}, \quad M_0 = 4 \pi M_\odot \left( \frac{R_0}{\text{pc}} \right)^3 = 0.8230 \cdot 10^5 M_\odot, \quad (2.21)$$

$$Q(r) \equiv \frac{\rho(r)}{\sigma^3(r)} = 3 \sqrt{3} \frac{\rho(r)}{\langle v^2 \rangle^{\frac{3}{2}}(r)} = \frac{\sqrt{125}}{3 \pi^2} \frac{m^4}{\hbar^3} \frac{I_2^{\frac{5}{2}}(\nu(\xi))}{I_4^{\frac{3}{2}}(\nu(\xi))}. \quad (2.22)$$

In these expressions, we have systematically eliminated the energy scale  $T_0$  in terms of the central density  $\rho_0$  through eq.(2.17). Notice that  $Q(r)$  turns to be independent of  $T_0$  and therefore of  $\rho_0$ .

We define the core size  $r_h$  of the halo by analogy with the Burkert density profile as

$$\frac{\rho(r_h)}{\rho_0} = \frac{1}{4}, \quad r_h = l_0 \xi_h. \quad (2.23)$$

It must be noticed that the surface density

$$\Sigma_0 \equiv r_h \rho_0, \quad (2.24)$$

is found nearly **constant** and independent of luminosity in different galactic systems (spirals, dwarf irregular and spheroidals, elliptics) spanning over 14 magnitudes in luminosity and over different Hubble types. More precisely, all galaxies seem to have the same value for  $\Sigma_0$ , namely  $\Sigma_0 \simeq 120 M_\odot/\text{pc}^2$  up to 10% – 20% [14, 18, 34]. It is remarkable that at the same time other important structural quantities as  $r_h$ ,  $\rho_0$ , the baryon-fraction and the galaxy mass vary orders of magnitude from one galaxy to another.

The constancy of  $\Sigma_0$  seems unlikely to be a mere coincidence and probably reflects a physical scaling relation between the mass and halo size of galaxies. It must be stressed that  $\Sigma_0$  is the only dimensionful quantity which is constant among the different galaxies.

It is then useful to take here the dimensionful quantity  $\Sigma_0$  as physical scale to express the galaxy magnitudes in the Thomas-Fermi approach. That is, we replace the central density  $\rho_0$  in the above galaxy magnitudes eqs.(2.14)-(2.21) in terms of  $\Sigma_0$  eq.(2.24) with the following results

$$l_0 = \left( \frac{9 \pi}{2^9} \right)^{\frac{1}{5}} \left( \frac{\hbar^6}{G^3 m^8} \right)^{\frac{1}{5}} \left[ \frac{\xi_h I_2(\nu_0)}{\Sigma_0} \right]^{\frac{1}{5}} = 4.2557 [\xi_h I_2(\nu_0)]^{\frac{1}{5}} \left( \frac{2 \text{ keV}}{m} \right)^{\frac{8}{5}} \left( \frac{120 M_\odot}{\Sigma_0 \text{ pc}^2} \right)^{\frac{1}{5}} \text{ pc}, \quad (2.25)$$

$$T_0 = \left( 18 \pi^6 \frac{\hbar^6 G^2}{m^3} \right)^{\frac{1}{5}} \left[ \frac{\Sigma_0}{\xi_h I_2(\nu_0)} \right]^{\frac{4}{5}} = \frac{7.12757 \cdot 10^{-3}}{[\xi_h I_2(\nu_0)]^{\frac{4}{5}}} \left( \frac{2 \text{ keV}}{m} \right)^{\frac{3}{5}} \left( \frac{\Sigma_0 \text{ pc}^2}{120 M_\odot} \right)^{\frac{4}{5}} \text{ K}, \quad (2.26)$$

and

$$r = 4.2557 \xi [\xi_h I_2(\nu_0)]^{\frac{1}{5}} \left( \frac{2 \text{ keV}}{m} \right)^{\frac{8}{5}} \left( \frac{120 M_\odot}{\Sigma_0 \text{ pc}^2} \right)^{\frac{1}{5}} \text{ pc}, \quad (2.27)$$

$$\rho(r) = \left( \frac{2^9 G^3 m^8}{9 \pi \hbar^6} \right)^{\frac{1}{5}} \left[ \frac{\Sigma_0}{\xi_h I_2(\nu_0)} \right]^{\frac{6}{5}} I_2(\nu(\xi)) = 18.1967 \frac{I_2(\nu(\xi))}{[\xi_h I_2(\nu_0)]^{\frac{6}{5}}} \left( \frac{m}{2 \text{ keV}} \right)^{\frac{8}{5}} \left( \frac{\Sigma_0 \text{ pc}^2}{120 M_\odot} \right)^{\frac{6}{5}} \frac{M_\odot}{\text{pc}^3}, \quad (2.28)$$

$$M(r) = 4 \pi \left( \frac{9 \pi \hbar^6}{2^9 G^3 m^8} \right)^{\frac{2}{5}} \left[ \frac{\Sigma_0}{\xi_h I_2(\nu_0)} \right]^{\frac{3}{5}} \xi^2 |\nu'(\xi)| = \frac{27312 \xi^2}{[\xi_h I_2(\nu_0)]^{\frac{3}{5}}} |\nu'(\xi)| \left( \frac{2 \text{ keV}}{m} \right)^{\frac{16}{5}} \left( \frac{\Sigma_0 \text{ pc}^2}{120 M_\odot} \right)^{\frac{3}{5}} M_\odot, \quad (2.29)$$

$$\sigma^2(r) = \frac{11.0402}{[\xi_h I_2(\nu_0)]^{\frac{4}{5}}} \frac{I_4(\nu(\xi))}{I_2(\nu(\xi))} \left( \frac{2 \text{ keV}}{m} \right)^{\frac{8}{5}} \left( \frac{\Sigma_0 \text{ pc}^2}{120 M_\odot} \right)^{\frac{4}{5}} \left( \frac{\text{km}}{\text{s}} \right)^2, \quad (2.30)$$

$$P(r) = \frac{8\pi}{5} G \left[ \frac{\Sigma_0}{\xi_h I_2(\nu_0)} \right]^2 I_4(\nu(\xi)) = \frac{200.895}{[\xi_h I_2(\nu_0)]^2} I_4(\nu(\xi)) \left( \frac{\Sigma_0 \text{ pc}^2}{120 M_\odot} \right)^2 \frac{M_\odot}{\text{pc}^3} \left( \frac{\text{km}}{\text{s}} \right)^2. \quad (2.31)$$

For a fixed value of the surface density  $\Sigma_0$ , the solutions of the Thomas-Fermi eqs.(2.16) are parametrized by a single parameter: the dimensionless chemical potential at the origin  $\nu_0$ . The value of  $\nu_0$  at fixed  $\Sigma_0$  can be determined by the value of the halo galaxy mass  $M(r_h)$  obtained from eq.(2.29) at  $r = r_h$ .

$$M_h \equiv M(r_h) = \frac{27312 \xi_h^{\frac{7}{5}}}{[I_2(\nu_0)]^{\frac{3}{5}}} |\nu'(\xi_h)| \left( \frac{2 \text{ keV}}{m} \right)^{\frac{16}{5}} \left( \frac{\Sigma_0 \text{ pc}^2}{120 M_\odot} \right)^{\frac{3}{5}} M_\odot. \quad (2.32)$$

Also, at fixed surface density  $\Sigma_0$ , the effective temperature  $T_0$  is only a function of  $\nu_0$ .

It is useful to introduce the rescaled dimensionless variables

$$\begin{aligned} \hat{r}_h &\equiv r_h \left( \frac{m}{2 \text{ keV}} \right)^{\frac{8}{5}} \left( \frac{\Sigma_0 \text{ pc}^2}{120 M_\odot} \right)^{\frac{1}{5}}, & \hat{M}_h &\equiv M_h \left( \frac{m}{2 \text{ keV}} \right)^{\frac{16}{5}} \left( \frac{120 M_\odot}{\Sigma_0 \text{ pc}^2} \right)^{\frac{3}{5}}, & \hat{T}_0 &\equiv T_0 \frac{2 \text{ keV}}{m} \left( \frac{120 M_\odot}{\Sigma_0 \text{ pc}^2} \right)^{\frac{4}{5}} \\ \hat{\nu}_0 &\equiv \nu_0 + 4 \ln \left( \frac{m}{2 \text{ keV}} \right), & \hat{\sigma}^2(r) &\equiv \sigma^2(r) \left( \frac{m}{2 \text{ keV}} \right)^{\frac{8}{5}} \left( \frac{120 M_\odot}{\Sigma_0 \text{ pc}^2} \right)^{\frac{4}{5}}, \end{aligned} \quad (2.33)$$

We display in Table I the corresponding values of the halo mass  $\hat{M}_h$ , the effective temperature  $\hat{T}_0$  and the chemical potential at the origin  $\nu_0$  in the whole galaxy mass range, from large diluted galaxies till small ultracompact galaxies.

The circular velocity  $v_c(r)$  is defined through the virial theorem as

$$v_c(r) \equiv \sqrt{\frac{G M(r)}{r}}, \quad (2.34)$$

and it is directly related by eq.(2.8) to the derivative of the chemical potential as

$$v_c(r) = \sqrt{-\frac{r}{m} \frac{d\mu}{dr}} = \sqrt{-\frac{T_0}{m} \frac{d\nu}{d \ln \xi}}.$$

Expressing  $T_0$  in terms of the surface density  $\Sigma_0$  using eq.(2.26) we have for the circular velocity the explicit expression

$$v_c(r) = 5.2537 \frac{\sqrt{-\xi \nu'(\xi)}}{[\xi_h I_2(\nu_0)]^{\frac{2}{5}}} \left( \frac{2 \text{ keV}}{m} \right)^{\frac{4}{5}} \left( \frac{\Sigma_0 \text{ pc}^2}{120 M_\odot} \right)^{\frac{2}{5}} \frac{\text{km}}{\text{s}}. \quad (2.35)$$

and the rescaled circular velocity,

$$\hat{v}_c^2(r) \equiv v_c^2(r) \left( \frac{m}{2 \text{ keV}} \right)^{\frac{8}{5}} \left( \frac{120 M_\odot}{\Sigma_0 \text{ pc}^2} \right)^{\frac{4}{5}}.$$

Two important combinations of galaxy magnitudes are  $r \rho(r')$  and  $M(r)/[4\pi r^2]$ . From eqs. (2.13), (2.20), (2.25) and (2.28) we obtain

$$r \rho(r') = \Sigma_0 \frac{\xi I_2(\nu(\xi'))}{\xi_h I_2(\nu_0)}, \quad \frac{M(r)}{4\pi r^2} = \Sigma_0 \frac{|\nu'(\xi)|}{\xi_h I_2(\nu_0)}. \quad (2.36)$$

In particular, it follows that  $r_h \rho(0) = \Sigma_0$  reproducing the surface density as it must be. At a generic point  $r$  eqs.(2.36) provide expressions for a space dependent surface density. They are both proportional to  $\Sigma_0$  and differ from each other by factors of order one. Notice that  $\hbar$ ,  $G$  and  $m$  canceled out in these space dependent surface densities eqs.(2.36).

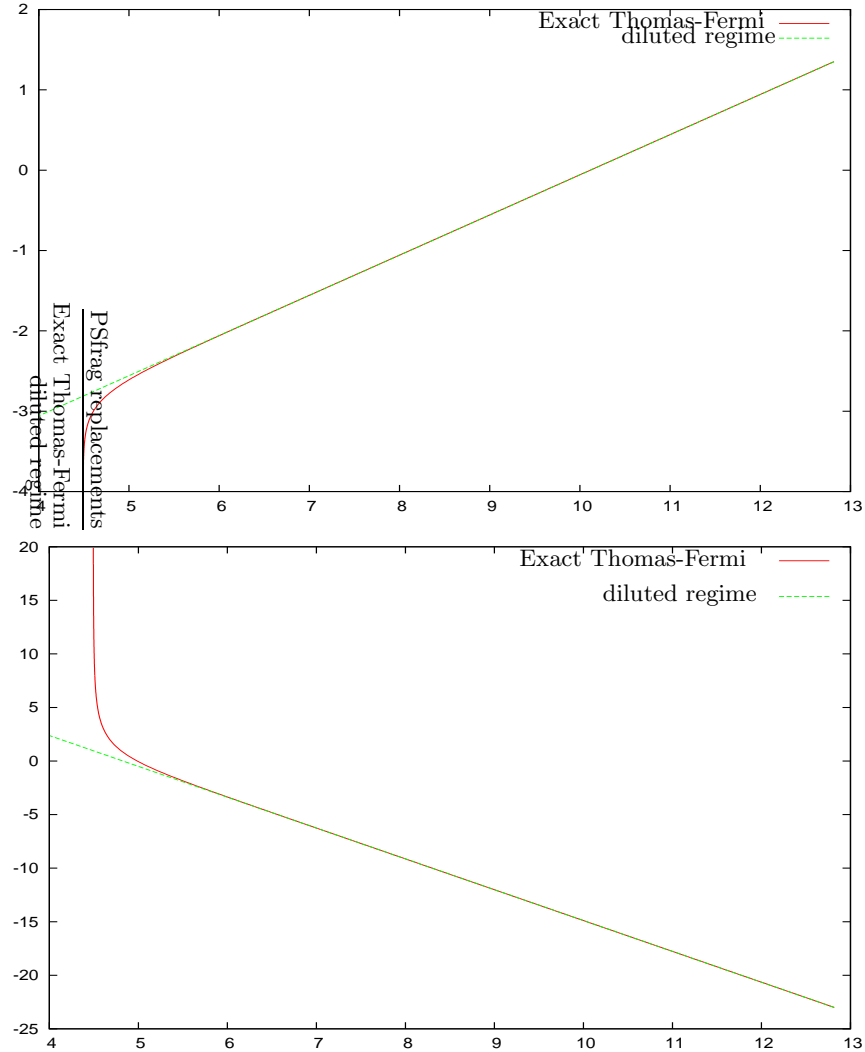


FIG. 1: Upper Panel: The ordinary logarithm of the effective temperature  $\hat{T}_0$  vs. the ordinary logarithm of the halo mass  $\hat{M}_h$ . We see that  $\hat{T}_0$  grows with  $\hat{M}_h$  following with precision the square-root of  $\hat{M}_h$  law as in the diluted regime eq.(2.37) of the Thomas-Fermi equations, except for  $\hat{M}_h < 3 \cdot 10^5 M_\odot$ ,  $\nu_0 > -1.8$ ,  $\hat{T}_0 < 0.005$  K which is near the quantum degenerate regime and corresponds to compact dwarf galaxies. The deviation from the scaling diluted regime is due to the quantum fermionic effects which become important for dwarf compact galaxies. Lower Panel. The dimensionless chemical potential at the origin  $\hat{\nu}_0$  vs. the ordinary logarithm of  $\hat{M}_h$ . We see that  $\hat{\nu}_0$  follows with precision the  $(5/4) \log \hat{M}_h$  law as in the diluted regime eq.(2.37) of the Thomas-Fermi equations. except near the degenerate regime for  $\hat{M}_h < 3 \cdot 10^5 M_\odot$ ,  $\nu_0 > -1.8$ ,  $\hat{T}_0 < 0.005$  K corresponding to compact dwarf galaxies.

### A. Galaxy properties in the diluted Boltzmann regime

In the diluted Boltzmann regime,  $\nu_0 \lesssim -5$ , the analytic expressions for the main galaxies magnitudes are given by:

$$M_h = 1.75572 \Sigma_0 r_h^2 \quad , \quad r_h = 68.894 \sqrt{\frac{M_h}{10^6 M_\odot} \frac{120 M_\odot}{\Sigma_0 \text{ pc}^2}} \text{ pc} \quad , \quad (2.37)$$

$$T_0 = 8.7615 \cdot 10^{-3} \sqrt{\frac{M_h}{10^6 M_\odot}} \frac{m}{2 \text{ keV}} \sqrt{\frac{\Sigma_0 \text{ pc}^2}{120 M_\odot}} \text{ K} \quad , \quad (2.38)$$

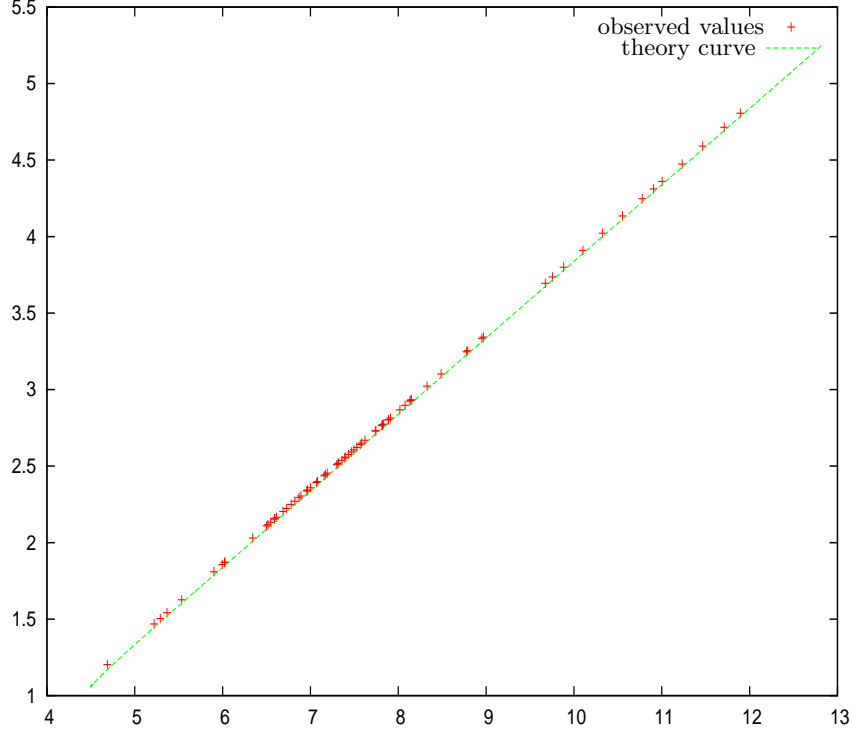


FIG. 2: The ordinary logarithm of the halo radius  $\hat{r}_h = r_h \left( \frac{\Sigma_0 \text{ pc}^2}{120 M_\odot} \right)^{\frac{1}{5}}$  vs. the ordinary logarithm of the halo mass  $\hat{M}_h = M_h \left( \frac{120 M_\odot}{\Sigma_0 \text{ pc}^2} \right)^{\frac{3}{5}}$ . We see that  $r_h$  follows with precision the square-root of  $M_h$  law as in the diluted regime eq.(2.37) of the Thomas-Fermi equations. In addition, the galaxy data confirm the proportionality factor in this scaling relation. The observational galaxy data for  $M_h$  and  $r_h$  are taken from Table 1 in [8] based on refs. [23], [28], [29], [30], [31]. The data are very well reproduced by the theoretical Thomas-Fermi curve. The errors of the data can be estimated to be about 10-20 %.

$\hat{M}_h$	$\hat{T}_0$	$\nu_0 = \frac{\mu(0)}{T_0}$
$6.56 \cdot 10^{12} M_\odot$	22.4 K	-23
$6.45 \cdot 10^{11} M_\odot$	7.04 K	-20.1
$6.34 \cdot 10^{10} M_\odot$	2.21 K	-17.2
$4.9 \cdot 10^9 M_\odot$	0.613 K	-14
$2.16 \cdot 10^8 M_\odot$	0.129 K	-10.1
$1.55 \cdot 10^7 M_\odot$	0.0344 K	-6.8
$3.67 \cdot 10^6 M_\odot$	0.0168 K	-5
$1.66 \cdot 10^6 M_\odot$	0.0112 K	-4
$1.21 \cdot 10^5 M_\odot$	0.00278 K	-0.4
$9.73 \cdot 10^4 M_\odot$	0.00241 K	0
$6.31 \cdot 10^4 M_\odot$	0.00173 K	1
$4.06 \cdot 10^4 M_\odot$	0.00101 K	3
$3.48 \cdot 10^4 M_\odot$	$6.82 \cdot 10^{-4}$ K	5
$3.19 \cdot 10^4 M_\odot$	$3.63 \cdot 10^{-4}$ K	10
$3.12 \cdot 10^4 M_\odot$	$1.84 \cdot 10^{-4}$ K	20
$\hat{M}_h^{min} = 3.10 \cdot 10^4 M_\odot$	0	$+\infty$

TABLE I: Corresponding values of the halo mass  $\hat{M}_h$ , the effective temperature  $\hat{T}_0$  and the chemical potential at the origin  $\nu_0$  for WDM galaxies covering the whole range from large diluted galaxies till small ultracompact galaxies.

$$\rho(r) = 5.19505 \left( \frac{M_h}{10^4 M_\odot} \frac{\Sigma_0 \text{ pc}^2}{120 M_\odot} \right)^{\frac{3}{4}} \left( \frac{m}{2 \text{ keV}} \right)^4 e^{\nu(\xi)} \frac{M_\odot}{\text{pc}^3}, \quad (2.39)$$

$$\sigma^2(r) = 33.927 \sqrt{\frac{M_h}{10^6 M_\odot} \frac{\Sigma_0 \text{ pc}^2}{120 M_\odot}} \left( \frac{\text{km}}{\text{s}} \right)^2, \quad (2.40)$$

$$v_c^2(r) = 33.9297 \sqrt{\frac{M_h}{10^6 M_\odot} \frac{\Sigma_0 \text{ pc}^2}{120 M_\odot}} \left| \frac{d\nu(\xi)}{d \ln \xi} \right| \left( \frac{\text{km}}{\text{s}} \right)^2, \quad v_c^2(r_h) = 62.4292 \sqrt{\frac{M_h}{10^6 M_\odot} \frac{\Sigma_0 \text{ pc}^2}{120 M_\odot}} \left( \frac{\text{km}}{\text{s}} \right)^2 \quad (2.41)$$

$$M(r) = 7.88895 \left| \frac{d\nu(\xi)}{d \ln \xi} \right| \frac{r}{\text{pc}} \sqrt{\frac{M_h}{10^6 M_\odot} \frac{\Sigma_0 \text{ pc}^2}{120 M_\odot}}. \quad (2.42)$$

In addition,  $M_h$  and  $T_0$  scale as functions of the fugacity at the center  $z_0 = e^{\nu_0}$ :

$$M_h \equiv M(r_h) = \frac{67014.6}{z_0^{\frac{4}{5}}} \left( \frac{2 \text{ keV}}{m} \right)^{\frac{16}{5}} \left( \frac{\Sigma_0 \text{ pc}^2}{120 M_\odot} \right)^{\frac{3}{5}} M_\odot, \quad (2.43)$$

$$T_0 = \frac{2.2681 \cdot 10^{-3}}{z_0^{\frac{2}{5}}} \left( \frac{2 \text{ keV}}{m} \right)^{\frac{3}{5}} \left( \frac{\Sigma_0 \text{ pc}^2}{120 M_\odot} \right)^{\frac{4}{5}} \text{ K}. \quad (2.44)$$

Therefore, **all** these galaxy magnitudes **scale** as functions of each other.

For the equation of state and the phase space density we find the expressions

$$P(r) = 5.57359 \cdot 10^3 \left( \frac{M_h}{10^6 M_\odot} \frac{\Sigma_0 \text{ pc}^2}{120 M_\odot} \right)^{\frac{5}{4}} \left( \frac{m}{2 \text{ keV}} \right)^4 e^{\nu(\xi)} \frac{M_\odot}{\text{pc}^3} \left( \frac{\text{km}}{\text{s}} \right)^2, \quad (2.45)$$

$$P_0 \equiv P(0) = 59.097 \left( \frac{\Sigma_0 \text{ pc}^2}{120 M_\odot} \right)^2 \frac{M_\odot}{\text{pc}^3} \left( \frac{\text{km}}{\text{s}} \right)^2, \quad (2.46)$$

$$Q(r) = 2.031796 \left( \frac{m}{2 \text{ keV}} \right)^4 e^{\nu(\xi)} \text{ keV}^4, \quad Q(0) = 1.2319 \left( \frac{10^5 M_\odot}{M_h} \right)^{\frac{5}{4}} \left( \frac{\Sigma_0 \text{ pc}^2}{120 M_\odot} \right)^{\frac{3}{4}} \text{ keV}^4. \quad (2.47)$$

These equations are accurate for  $M_h \gtrsim 10^6 M_\odot$ . We see that they exhibit a **scaling** behaviour for  $r_h$ ,  $T_0$ ,  $Q(0)$ ,  $\sigma^2(0)$  and  $v_c^2(r_h)$  as functions of  $M_h$ .

We see from eqs.(2.37) and (2.40) that  $T_0$  and  $m \sigma^2(0)$  only differ by purely numerical factors reflecting the equipartition of kinetic energy. More precisely, it follows from eqs.(2.37) and (2.40) that

$$\frac{m}{2} \langle v^2(0) \rangle = \frac{3}{2} m \sigma^2(0) = \frac{3}{2} T_0, \quad (2.48)$$

which shows that in the diluted regime the self-gravitating WDM gas behaves as an **inhomogeneous perfect gas** as we will discuss in the next section.

We plot in figs. 1 and 2, the dimensionless effective temperature  $\hat{T}_0$ , the chemical potential at the origin  $\hat{\nu}_0$  and the normalized halo radius  $\hat{r}_h$  as functions of the halo mass  $\hat{M}_h$  as defined by eqs.(2.33). We also depict in fig. 2 the galaxy observations from different sets of data from refs. [23], [28], [29], [30], [31]. All data are well reproduced by our theoretical Thomas-Fermi results. The errors of the data can be estimated to be about 10-20 %.

The characteristic temperature  $\hat{T}_0$  monotonically grows with the halo mass  $\hat{M}_h$  of the galaxy as shown by fig. 1 and eq.(2.43) following with good precision the square root of  $\hat{M}_h$  eq.(2.37).

We see that the whole set of scaling behaviours of the diluted regime eqs. (2.37)-(2.43) are **very accurate** except near the degenerate regime for halo masses  $\hat{M}_h < 3 \cdot 10^5 M_\odot$ . The deviation from the diluted scaling regime for

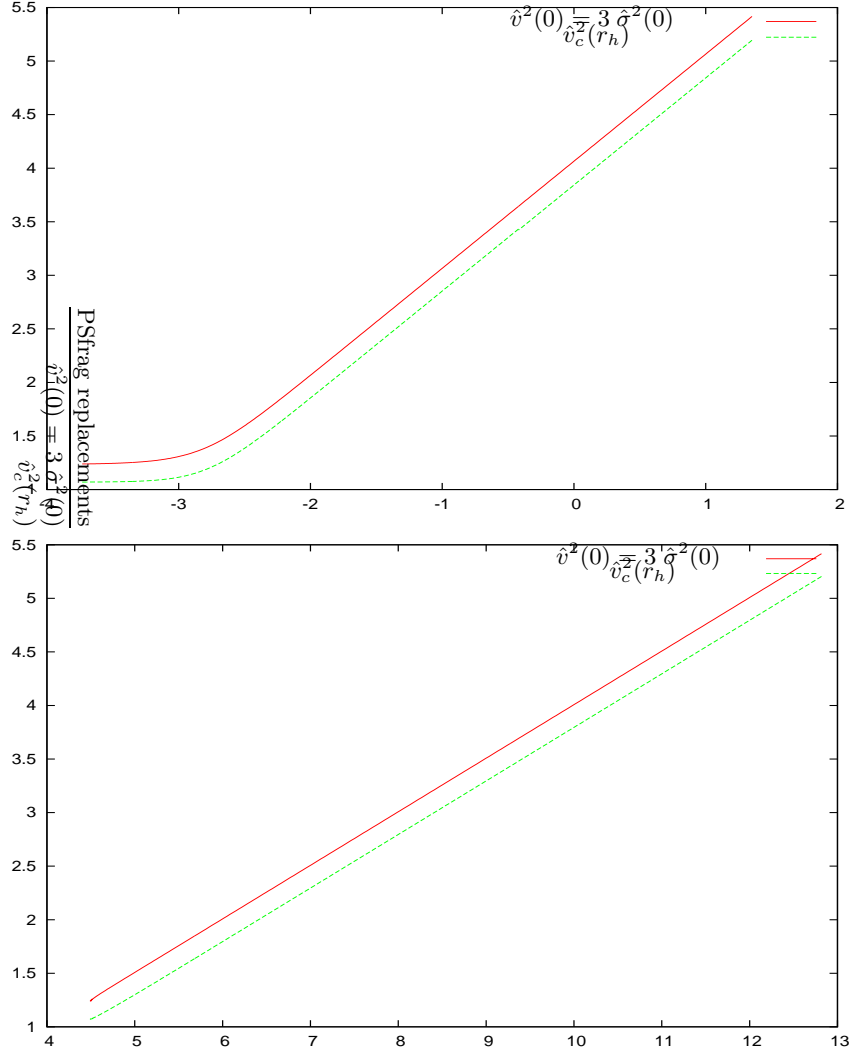


FIG. 3: The ordinary logarithm of the velocity dispersion at the origin  $\hat{v}^2(0) = 3 \hat{\sigma}^2(0)$  and the ordinary logarithm of the circular velocity at the halo radius  $\hat{v}_c^2(r_h)$  vs.  $\log_{10} \hat{T}_0$  in the upper panel and vs.  $\log_{10} \hat{M}_h$  in the lower panel. Notice the unit slope in the upper panel curves as functions of  $\hat{T}_0$  according to eq.(3.3) in the diluted regime, and the one-half slope in the lower panel curves as functions of  $\hat{M}_h$  following eqs.(2.40)-(2.41) in the diluted regime. The deviation from the diluted scaling regime near the degenerate regime is manifest as function of  $\hat{T}_0$  (upper panel) while it is imperceptible as function of  $\hat{M}_h$  (lower panel).

$\hat{M}_h < 3 \cdot 10^5 M_\odot$  accounts for the quantum fermionic effects in the dwarf compact galaxies obtained in our Thomas-Fermi approach.

It must be stressed that the scaling relations eqs.(2.37)-(2.47) are a consequence solely of the self-gravitating interaction of the fermionic WDM. Galaxy data verify the exponent and the amplitude factor in these scaling as shown in fig. 2 for the square root scaling relation eq.(2.37).

It is highly remarkable that our theoretical results **reproduce** the observed DM halo properties with **good precision**.

The opposite limit,  $\nu_0 \gtrsim 1$ , is the quantum regime corresponding to compact WDM fermions. In particular, in the degenerate limit  $\nu_0 \rightarrow \infty$ , the galaxy mass and halo radius take their **minimum** values

$$r_h^{min} = 11.3794 \left( \frac{2 \text{ keV}}{m} \right)^{\frac{8}{5}} \left( \frac{120 M_\odot}{\Sigma_0 \text{ pc}^2} \right)^{\frac{1}{5}} \text{ pc},$$

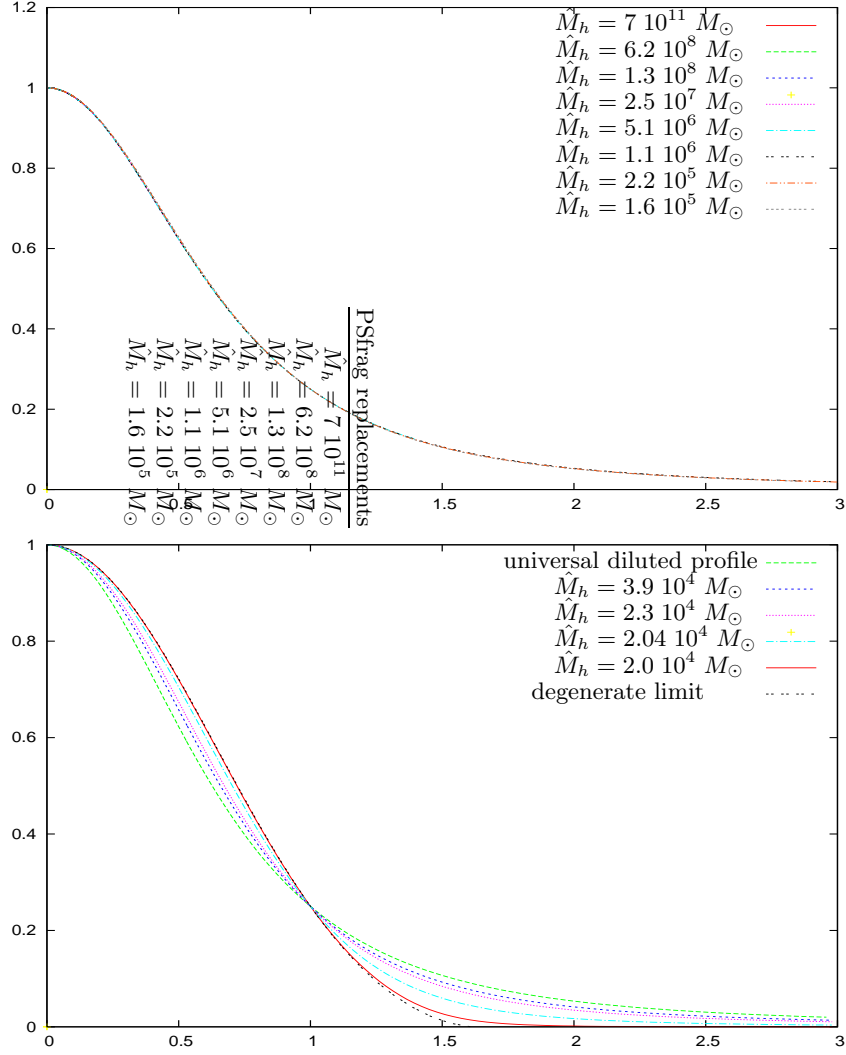


FIG. 4: Normalized density profiles  $\rho(r)/\rho(0)$  as functions of  $r/r_h$ . We display in the upper panel the profiles for galaxy masses in the diluted regime  $1.4 \cdot 10^5 M_\odot < \hat{M}_h < 7.5 \cdot 10^{11} M_\odot$ ,  $-1.5 > \nu_0 > -20.78$  which **all** provide the **same universal** density profile. We display in the lower panel the profiles for galaxy masses  $M_h^{min} = 30999 (2 \text{ keV}/m)^{\frac{16}{5}} M_\odot \leq \hat{M}_h < 3.9 \cdot 10^4 M_\odot$ ,  $1 < \nu_0 < \infty$  which are near the quantum degenerate regime and exhibit shrinking density profiles for decreasing galaxy mass. For comparison, we also plot in the lower figure the universal profile in the diluted regime.

$$M_h^{min} = 30998.7 \left( \frac{2 \text{ keV}}{m} \right)^{\frac{16}{5}} \left( \frac{\Sigma_0 \text{ pc}^2}{120 M_\odot} \right)^{\frac{3}{5}} M_\odot, \quad (2.49)$$

while the phase-space density  $Q(r)$  takes its **maximum** value

$$Q_h^{max} = 16 \frac{\sqrt{125}}{3 \pi^2} \left( \frac{m}{2 \text{ keV}} \right)^4 \text{ keV}^4 = 6.04163 \left( \frac{m}{2 \text{ keV}} \right)^4 \text{ keV}^4. \quad (2.50)$$

From the minimum value of the galaxy mass  $M_h^{min}$  we derive a lower bound for the WDM particle mass  $m$

$$m \geq m_{min} \equiv 1.387 \text{ keV} \left( \frac{10^5 M_\odot}{M_h} \right)^{\frac{5}{16}} \left( \frac{\Sigma_0 \text{ pc}^2}{120 M_\odot} \right)^{\frac{3}{16}} \quad (2.51)$$

From the minimal known halo mass  $M_h = 3.9 \cdot 10^4 M_\odot$  for Willman I (see Table 1 in [8]) we obtain the lower bound

$$m \geq 1.86 \text{ keV} \quad \text{for Dirac fermions} \quad , \quad m \geq 2.21 \text{ keV} \quad \text{for Majorana fermions} \quad .$$

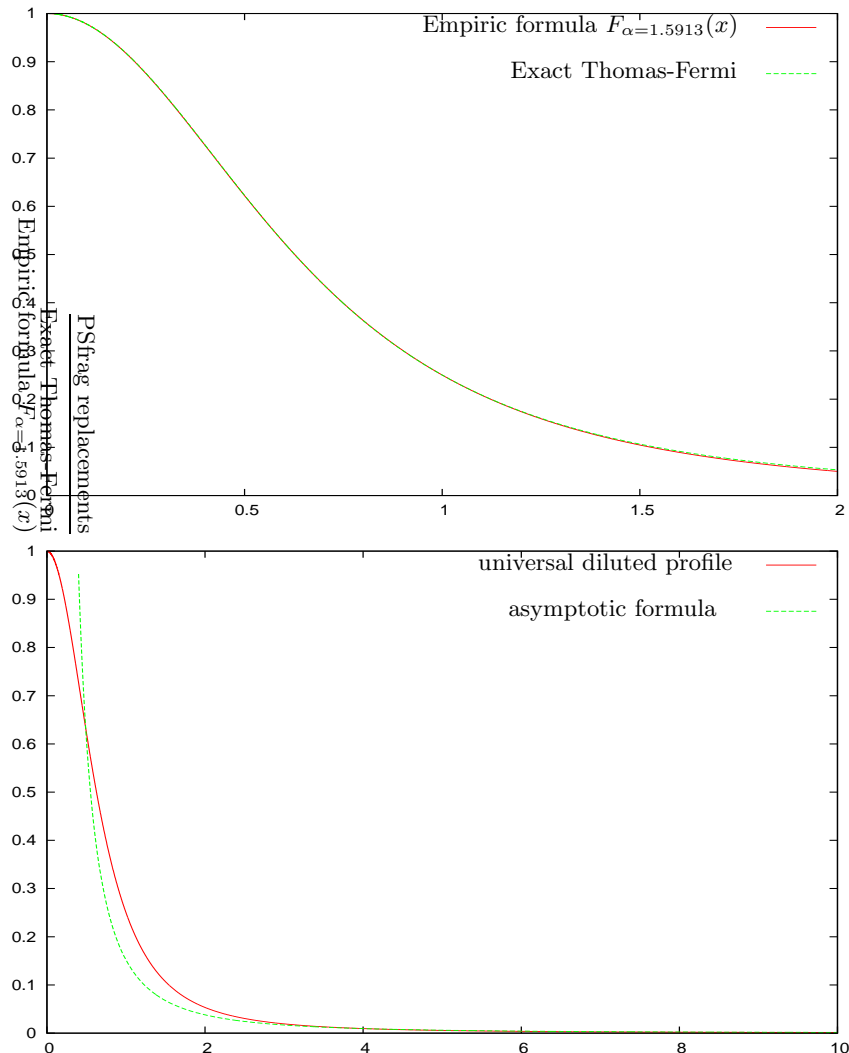


FIG. 5: Upper panel. The universal density profile  $\rho(r)/\rho(0)$  obtained from the Thomas-Fermi equations plotted vs.  $x = \frac{r}{r_h}$  and its fitting formula (3.1) for the best fit value  $\alpha = 1.5913$ . Lower panel. The universal density profile  $F(x)$  obtained from the Thomas-Fermi equations vs.  $x = r/r_h$  and its asymptotic form  $F_{asy}(x)$  given by eq.(3.2). For  $x \gtrsim 3$ ,  $F_{asy}(x)$  becomes a very good approximation to  $F(x)$ .

### III. DENSITY AND VELOCITY DISPERSION. UNIVERSAL AND NON-UNIVERSAL PROFILES

It is illuminating to normalize the density profiles as  $\rho(r)/\rho(0)$  and plot them as functions of  $r/r_h$ . We find that these normalized profiles are **universal** functions of  $x \equiv r/r_h$  in the diluted regime as shown in fig. 4. This universality is valid for **all** galaxy masses  $\hat{M}_h > 10^5 M_\odot$ .

No analytic form is available for the profile  $\rho(r)$  obtained from the resolution of the Thomas-Fermi equations (2.16). The universal profile  $F(x) = \rho(r)/\rho(0)$  can be fitted with precision by the simple formula

$$F_\alpha(x) = \frac{1}{\left[1 + \left(4^{\frac{1}{\alpha}} - 1\right) x^2\right]^\alpha}, \quad x = \frac{r}{r_h}, \quad \alpha = 1.5913. \quad (3.1)$$

The value  $\alpha = 1.5913$  provides the best fit. We plot in fig. 5  $\rho(r)/\rho(0)$  from the Thomas-Fermi equations (2.16) and the precise fitting formula  $F_{\alpha=1.5913}(x)$ . The fit is particularly precise for  $r < 2 r_h$ .

Our theoretical density profiles and rotation curves obtained from the Thomas-Fermi equations remarkably agree with observations for  $r \lesssim r_h$ , for all galaxies in the diluted regime [13]. This indicates that WDM is thermalized in the internal regions  $r \lesssim r_h$  of galaxies.

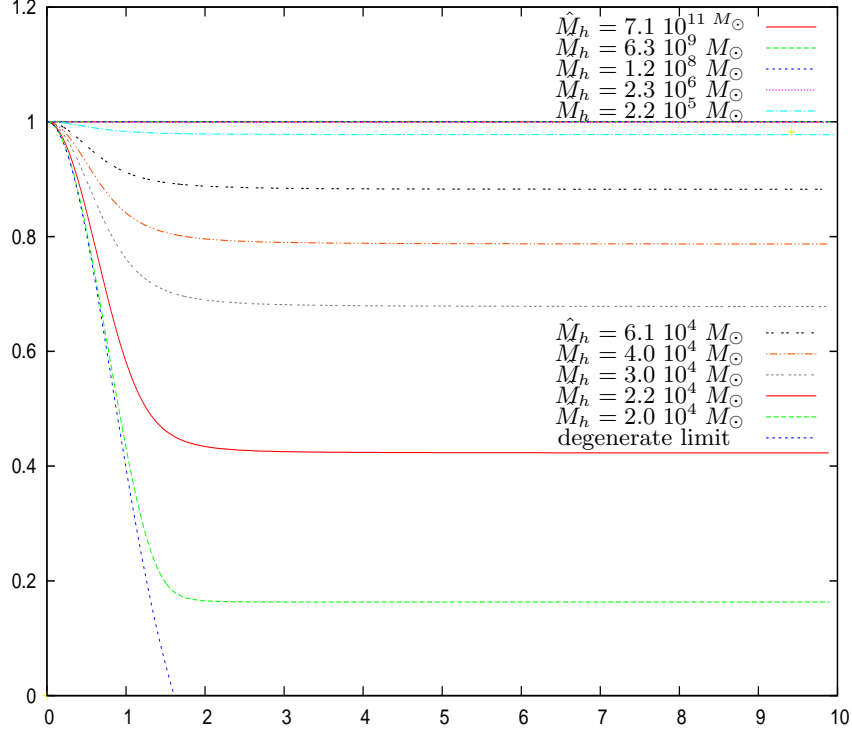


FIG. 6: Normalized velocity dispersion profiles  $\sigma^2(r)/\sigma^2(0)$  as functions of  $x = r/r_h$ . All velocity profiles in the diluted regime for galaxy masses  $\hat{M}_h > 2.3 \cdot 10^6 M_\odot$ ,  $\nu_0 < -5$  fall into the same **constant universal** profile corresponding to a perfect but inhomogeneous self-gravitating WDM gas describing large and diluted galaxies. The velocity profiles for smaller galaxy masses  $1.6 \cdot 10^6 M_\odot > \hat{M}_h > \hat{M}_{h,min} = 3.10 \cdot 10^4 M_\odot$  do depend on  $x$  and yield decreasing velocity dispersions for decreasing galaxy masses, accounting for the quantum fermionic effects which become important in this range of galaxy masses (WDM compact dwarf galaxies).

The theoretical profile  $\rho(r)/\rho(0)$  and the precise fit  $F_{\alpha=1.5913}(x)$  cannot be used for  $x \gg 1$  where they decay as a power  $\simeq 3.2$  which is a too large number to reproduce the observations.

The universal density profile  $\rho(r)/\rho(0)$  is obtained theoretically in the diluted Boltzmann regime. In such regime the density profile decreases for large  $x \gg 1$  as  $\sim 1/x^2$ . More precisely, we find the asymptotic behaviour

$$F(x) \stackrel{x \gg 1}{\simeq} F_{asy}(x) \equiv \frac{0.151869}{x^2} \left[ 1 + \mathcal{O}\left(\frac{1}{\sqrt{x}}\right) \right]. \quad (3.2)$$

We plot in fig. 5  $F(x)$  and its asymptotic behaviour  $F_{asy}(x)$  vs.  $x$ . We see that  $F_{asy}(x)$  becomes a very good approximation to  $F(x)$  for  $x \gtrsim 3$ . When  $F(x)$  behaves as  $\sim 1/x^2$  the circular velocity for these theoretical density profiles becomes constant as shown in [13].

For galaxy masses  $\hat{M}_h < 10^5 M_\odot$ , near the quantum degenerate regime, the normalized density profiles  $\rho(r)/\rho(0)$  are not anymore universal and depend on the galaxy mass.

As we can see in fig. 4 the density profile shape changes fastly when the galaxy mass decreases only by a factor seven from  $\hat{M}_h = 1.4 \cdot 10^5 M_\odot$  to the minimal galaxy mass  $\hat{M}_{h,min} = 3.10 \cdot 10^4 M_\odot$ . In this narrow range of galaxy masses the density profiles shrink from the universal profile till the degenerate profile as shown in fig. 4. Namely, these dwarf galaxies are more compact than the larger diluted galaxies.

We display in fig. 6 the normalized velocity dispersion profiles  $\sigma^2(r)/\sigma^2(0)$  as functions of  $x = r/r_h$ . Again, we see that these profiles are **universal and constant**, i. e. independent of the galaxy mass in the diluted regime for  $\hat{M}_h > 2.3 \cdot 10^6 M_\odot$ ,  $\nu_0 < -5$ ,  $T_0 > 0.017$  K. The constancy of  $\sigma^2(r) = \sigma^2(0)$  in the diluted regime implies that the equation of state is that of a perfect but inhomogeneous WDM gas. Indeed, from eq.(2.48)

$$\sigma^2(r) = \sigma^2(0) = \frac{T_0}{m}, \quad (3.3)$$

and eq.(2.6) implies for the WDM diluted galaxies the perfect gas equation of state (4.3) where both the pressure  $P(r)$  and the density  $\rho(r)$  depend on the coordinates.

For smaller galaxy masses  $1.6 \cdot 10^6 M_\odot > \hat{M}_h > \hat{M}_{h,min}$ , the velocity profiles do depend on  $r$  and yield decreasing velocity dispersions for decreasing galaxy masses. Namely, the deviation from the universal curves appears for  $\hat{M}_h < 10^6 M_\odot$  and we see that it precisely arises from the quantum fermionic effects which become important in such range of galaxy masses.

#### IV. THE EQUATION OF STATE OF WDM GALAXIES. CLASSICAL DILUTED AND COMPACT QUANTUM REGIMES.

The WDM galaxy equation of state is by definition the functional relation between the pressure  $P$  and the density  $\rho$ .

From eqs. (2.17) and (2.18) we obtain separately  $P$  and  $\rho$  at a point  $r$  as

$$\rho = \frac{m^{\frac{5}{2}}}{3 \pi^2 \hbar^3} (2 T_0)^{\frac{3}{2}} I_2(\nu) \quad , \quad P = \frac{m^{\frac{3}{2}}}{15 \pi^2 \hbar^3} (2 T_0)^{\frac{5}{2}} I_4(\nu) . \quad (4.1)$$

These equations express parametrically, through the parameter  $\nu$ , the pressure  $P$  as a function of the density  $\rho$  and therefore provide the WDM galaxy equation of state.

For fermionic WDM in thermal equilibrium  $I_2(\nu)$  and  $I_4(\nu)$  are given as integrals of the Fermi–Dirac distribution function in eq.(2.15). For WDM out of thermal equilibrium eq.(4.1) is always valid but  $I_2(\nu)$  and  $I_4(\nu)$  should be expressed as integrals of the corresponding out of equilibrium distribution function. In the out of equilibrium case  $T_0$  is just the characteristic scale in the out of equilibrium distribution function  $f_{out}(E) = \Psi_{out}(E/T_0)$ . For the relevant galaxy physical magnitudes, the Fermi–Dirac distribution gives similar results than the out of equilibrium distribution functions [8].

In the two WDM galaxy regimes, classical diluted regime, and degenerate quantum regime, we can eliminate  $\nu$  in eqs.(4.1) and obtain  $P$  as a function of  $\rho$  in close form. Let us take the ratios  $P/\rho$  and  $P/\rho^{\frac{5}{3}}$  in eqs.(4.1):

$$\frac{P}{\rho} = \frac{2}{5} \frac{T_0}{m} \frac{I_4(\nu)}{I_2(\nu)} \quad , \quad \frac{P}{\rho^{\frac{5}{3}}} = \frac{\hbar^2}{5} \left( \frac{3 \pi^2}{m^4} \right)^{\frac{2}{3}} \frac{I_4(\nu)}{I_2^{\frac{5}{3}}(\nu)} . \quad (4.2)$$

In the diluted limit  $\nu \ll -1$  we have that

$$\frac{I_4(\nu)}{I_2(\nu)} \stackrel{\nu \ll -1}{\approx} \frac{5}{2}$$

and therefore we obtain for WDM in the diluted limit the local perfect gas equation of state:

$$P(r) = \frac{T_0}{m} \rho(r) \quad , \quad \text{WDM diluted galaxies} . \quad (4.3)$$

The local perfect WDM gas equation of state eq.(4.3) is precisely the equation of state of the Boltzmann self-gravitating gas [10].

In the degenerate limit  $\nu \gg 1$  we have that

$$\frac{I_4(\nu)}{I_2^{\frac{5}{3}}(\nu)} \stackrel{\nu \gg 1}{\approx} 1$$

and therefore  $P/\rho^{\frac{5}{3}}$  in eq.(4.2) becomes the degenerate fermionic equation of state at  $T_0 = 0$ ,

$$P = \frac{\hbar^2}{5} \left( \frac{3 \pi^2}{m^4} \right)^{\frac{2}{3}} \rho^{\frac{5}{3}} \quad , \quad \text{WDM degenerate quantum limit} . \quad (4.4)$$

Making explicit the dimensions, the WDM galaxy equation of state (4.1) becomes

$$\rho = 4.68591 \cdot 10^4 \left( \frac{T_0}{\text{K}} \right)^{\frac{3}{2}} I_2(\nu) \left( \frac{m}{2 \text{ keV}} \right)^{\frac{5}{2}} \frac{M_\odot}{\text{pc}^3} \quad , \quad P = 0.807603 \cdot 10^{-3} \left( \frac{T_0}{\text{K}} \right)^{\frac{5}{2}} I_4(\nu) \left( \frac{m}{2 \text{ keV}} \right)^{\frac{3}{2}} \frac{M_\odot}{\text{pc}^3} . \quad (4.5)$$

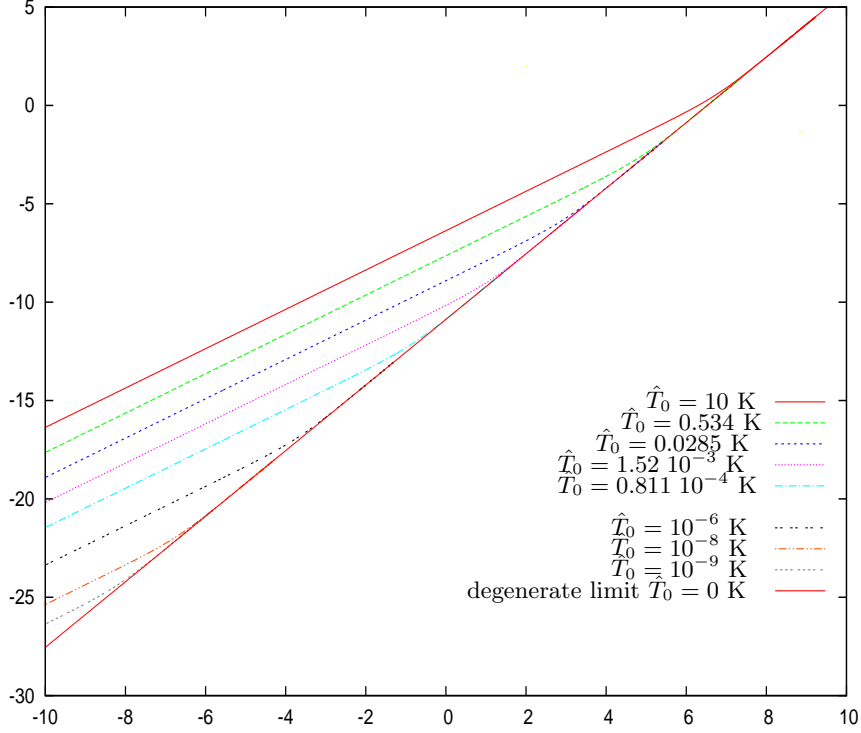


FIG. 7: The equation of state of WDM galaxies. Logarithmic plot of the galaxy pressure  $\bar{P}$  vs. the density  $\bar{\rho}$  as defined by eq.(4.6) for different values of the effective temperature  $T_0$ . For small density and growing  $T_0$ , the self-gravitating ideal WDM gas behaviour is obtained exhibiting straight lines with unit slope; this describes the physical state of large diluted galaxies  $\hat{M}_h > 2.3 \cdot 10^6 M_\odot$ ,  $\nu_0 < -5$ ,  $T_0 > 0.017$  K. For large density and decreasing temperature the fermionic quantum behaviour close to the degenerate state eq.(4.4) shows up as the steeper straight lines with slope approaching 5/3. In particular, the degenerate  $T_0 = 0$  state exhibits the slope 5/3 for all densities. The diluted classical regime and the degenerate regime are interpolated smoothly by the quantum behaviour corresponding to compact dwarf galaxies with  $1.6 \cdot 10^6 M_\odot > \hat{M}_h \geq \hat{M}_{h,min} = 3.10 \cdot 10^4 M_\odot$ ,  $\nu_0 > -4$ ,  $T_0 < 0.011$  K. For increasing  $T_0$  the curves move up. The larger is  $T_0$ , the larger is the value of the density  $\bar{\rho}$  where the quantum behaviour is attained.

Being the galaxies a nonrelativistic system,  $P$  turns to be much smaller than  $\rho$  when both are written in the same units where the speed of light is taken to be unit.

It is useful to introduce the rescaled dimensionless variables

$$\bar{\rho} \equiv \left( \frac{2 \text{ keV}}{m} \right)^{\frac{5}{2}} \frac{\text{pc}^3}{M_\odot} \rho = 4.68591 \cdot 10^4 \left( \frac{T_0}{\text{K}} \right)^{\frac{3}{2}} I_2(\nu) \quad , \quad \bar{P} \equiv \left( \frac{2 \text{ keV}}{m} \right)^{\frac{3}{2}} \frac{\text{pc}^3}{M_\odot} P = 0.807603 \cdot 10^{-3} \left( \frac{T_0}{\text{K}} \right)^{\frac{5}{2}} I_4(\nu) . \quad (4.6)$$

We plot in fig. 7 the ordinary logarithm of  $\bar{P}$  vs. the ordinary logarithm of  $\bar{\rho}$  for different values of  $T_0$ . For small density and for growing effective temperature, the self-gravitating ideal WDM gas behaviour eq.(4.3) of the diluted regime is obtained. On the contrary, for large density and for decreasing temperature the fermionic quantum behaviour close to the degenerate state eq.(4.4) shows up. That is, the straight lines with unit slope in fig. 7 describe the perfect WDM gas behaviour eq.(4.3), while the steeper straight lines with slope 5/3 describe the degenerate quantum behaviour eq.(4.4). We see that the diluted classical and degenerate regimes are interpolated smoothly by the quantum behaviour. For increasing  $T_0$  the curves in fig. 7 move up. The larger is  $T_0$ , the larger is the value of the density  $\bar{\rho}$  where the quantum behaviour is attained.

We plot in fig. 8 the pressure normalized to its value at the origin as a function of the density normalized to its value at the origin according to eqs.(4.1):

$$\frac{P}{P_0} = \frac{I_4(\nu)}{I_4(\nu_0)} \quad \text{vs.} \quad \frac{\rho}{\rho_0} = \frac{I_2(\nu)}{I_2(\nu_0)} . \quad (4.7)$$

The diluted and degenerate gas behaviours eq.(4.3) and (4.4) of WDM galaxies are explicitly seen in fig. 8. The

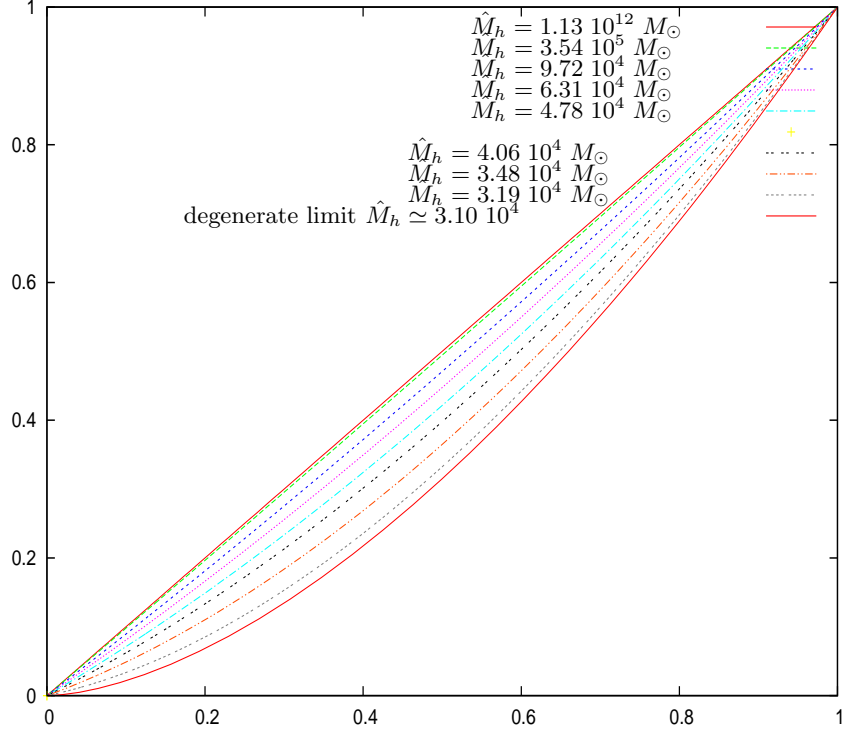


FIG. 8: The galaxy pressure  $P/P_0$  vs. the density  $\rho/\rho_0$ , where  $P_0$  and  $\rho_0$  are the pressure and the density at the origin, respectively defined by eq.(4.7). We see the WDM ideal gas behaviour (unit slope) in the diluted regime, that is for galaxy masses  $\hat{M}_h > 2.3 \cdot 10^6 M_\odot$ ,  $\nu_0 < -5$ ,  $T_0 > 0.017$  K. For smaller galaxy masses,  $1.6 \cdot 10^6 M_\odot > \hat{M}_h \geq \hat{M}_{h,min} = 3.10 \cdot 10^4 M_\odot$ ,  $\nu_0 > -4$ , the equation of state depends on the galaxy mass and becomes steeper corresponding to the quantum fermionic regime of dwarf galaxies. In the degenerate limit  $\nu_0 = \infty$  we obtain a 5/3 slope straight line. We see that the diluted and degenerate regimes are interpolated smoothly by the quantum behaviour.

diluted perfect gas behaviour appears for galaxy masses  $\hat{M}_h > 2.3 \cdot 10^6 M_\odot$ ,  $\nu_0 < -5$ ,  $T_0 > 0.017$  K. The degenerate gas behaviour shows up for the minimal mass galaxy  $\hat{M}_{h,min} = 3.10 \cdot 10^4 M_\odot$ ,  $T_0 = 0$ .

Besides the two limiting regimes, diluted and degenerate, we see from fig. 8 that the equation of state **does depend** on the galaxy mass for galaxy masses in the range  $1.6 \cdot 10^6 M_\odot > \hat{M}_h \geq \hat{M}_{h,min}$ ,  $\nu_0 > -4$ ,  $T_0 < 0.011$  K. This is a quantum regime, close to but not at, the degenerate limit. The equation of state in this quantum regime is steeper than in the degenerate limit.

We find that WDM galaxies exhibit two regimes: classical diluted and quantum compact (close to degenerate). WDM galaxies are diluted for  $\hat{M}_h > 2.3 \cdot 10^6 M_\odot$ ,  $\nu_0 < -5$ ,  $T_0 > 0.017$  K and they are quantum and compact for  $1.6 \cdot 10^6 M_\odot > \hat{M}_h \geq \hat{M}_{h,min}$ ,  $\nu_0 > -4$ ,  $T_0 < 0.011$  K. The degenerate limit  $T_0 = 0$  corresponds to the extreme quantum situation yielding a minimal galaxy size  $\hat{r}_{h,min}$  and mass  $\hat{M}_{h,min}$  given by eq.(2.49). The equation of state covering all regimes is given by eq. (4.1).

We therefore find an explanation for the universal density profiles and universal velocity profiles in diluted galaxies ( $\hat{M}_h \gtrsim 10^6 M_\odot$ ): these **universal properties** can be traced back to the perfect gas behaviour of the self-gravitating WDM gas summarized by the WDM equation of state (4.3). Notice that all these universal theoretical profiles well reproduce the observations for  $r \lesssim r_h$  [13].

For small galaxy masses,  $10^6 M_\odot \gtrsim \hat{M}_h \geq \hat{M}_{h,min} = 3.10 \cdot 10^4 M_\odot$  which correspond to chemical potentials at the origin  $\nu_0 \gtrsim -5$  and effective temperatures  $T_0 \lesssim 0.017$  K, the equation of state is galaxy mass dependent (see fig. 8) and the profiles are not anymore universal. These properties account to the quantum physics of the self-gravitating WDM fermions in the compact case close to the degenerate state.

Indeed, it will be extremely interesting to dispose of observations which could check these quantum effects in dwarf galaxies.

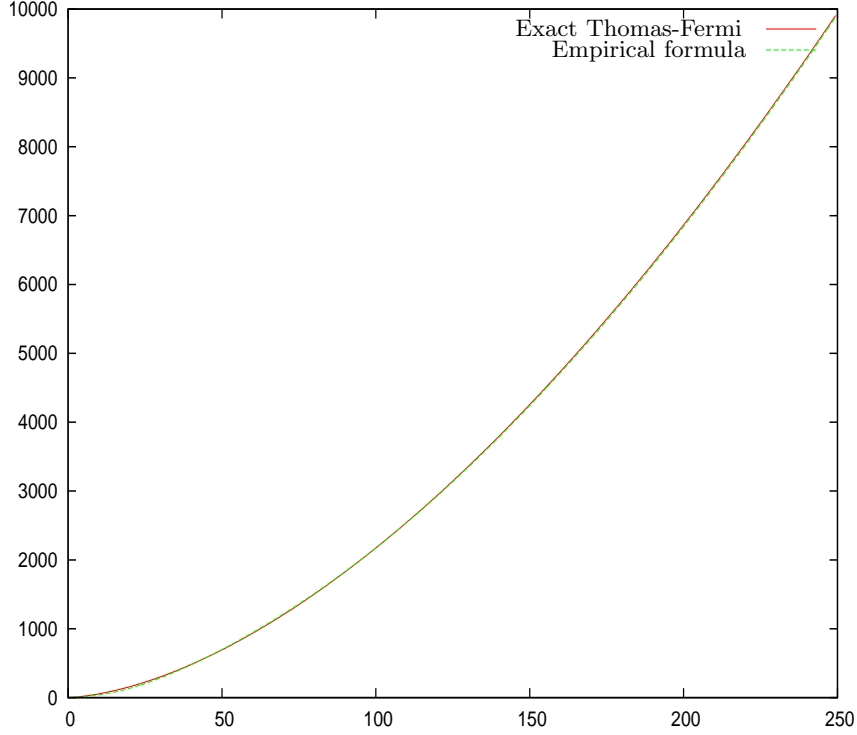


FIG. 9: The equation of state  $\tilde{P}$  vs.  $\tilde{\rho}$  obtained by solving the Thomas-Fermi eq.(2.3) and the empirical fit eqs.(4.9)-(4.10). The exact equation of state and the fitting formula cannot be distinguished at this resolution.

An useful empiric fit of the exact equation of state follows by expressing the pressure given by (4.1)

$$P = \frac{m^{\frac{3}{2}} (2 T_0)^{\frac{5}{2}}}{15 \pi^2 \hbar^3} \tilde{P} \quad \text{where} \quad \tilde{P} \equiv I_4(\nu) \quad (4.8)$$

as a function of

$$\tilde{\rho} \equiv \frac{3 \pi^2 \hbar^3}{m^{\frac{3}{2}} (2 T_0)^{\frac{3}{2}}} \rho = I_2(\nu) \quad (4.9)$$

We represent  $\tilde{P}$  as a function  $\tilde{\rho}$  through the simple function

$$\tilde{P} = \left(1 + \frac{3}{2} e^{-\beta_1 \tilde{\rho}}\right) \tilde{\rho}^{\frac{1}{3}} (5 - 2 e^{-\beta_2 \tilde{\rho}}) \quad (4.10)$$

that exactly fulfils the diluted and degenerate limiting behaviours (4.3) and (4.4), respectively. Eq.(4.10) best fits the exact values of  $\tilde{P}$  as a function  $\tilde{\rho}$  obtained by solving the Thomas-Fermi eq.(2.3) for

$$\beta_1 = 0.047098 \quad , \quad \beta_2 = 0.064492 . \quad (4.11)$$

In summary, we represent the equation of state as

$$P = \frac{m^{\frac{3}{2}} (2 T_0)^{\frac{5}{2}}}{15 \pi^2 \hbar^3} \left(1 + \frac{3}{2} e^{-\beta_1 \tilde{\rho}}\right) \tilde{\rho}^{\frac{1}{3}} (5 - 2 e^{-\beta_2 \tilde{\rho}})$$

where  $\tilde{\rho}$  is expressed in terms of  $\rho$  by eq.(4.9). We plot in fig. 9  $\tilde{P}$  vs.  $\tilde{\rho}$  obtained by solving the Thomas-Fermi eq.(2.3) and the empirical fit eq.(4.10). One can see that the fit turns to be excellent.

## V. THE DEPENDENCE ON THE WDM PARTICLE MASS IN THE DILUTED AND QUANTUM REGIMES

In the diluted limit the velocity dispersion is constant  $\sigma^2(r) = \sigma^2(0)$ , eq.(2.11) and eq.(3.3) lead to

$$\frac{d^2\mu}{dr^2} + \frac{2}{r} \frac{d\mu}{dr} = -4\pi G m \rho(r) \quad (5.1)$$

$$\rho(r) = \frac{1}{4} \left( \frac{2T_0}{\pi m} \right)^{\frac{3}{2}} m^4 \exp \left[ \frac{\mu(r)}{T_0} \right]. \quad (5.2)$$

In this diluted limit, the Thomas-Fermi equations (2.3) become the equations for a self-gravitating Boltzmann gas in thermal equilibrium.

Eq.(5.2) combined with the chemical potential expression (2.1) becomes the baryotropic equation

$$\rho(r) = \rho_0 e^{-\frac{m}{T_0} [\phi(r) - \phi(0)]}.$$

It is instructive to discuss from eq.(5.1) the dependence on the mass  $m$  of the WDM particle.

In the diluted regime,  $T_0$  and  $\mu(r)$  depend on  $m$ , while other magnitudes as  $\rho(r)$ ,  $M(r)$ ,  $\sigma^2(r)$ ,  $P(r)$ ,  $Q(r)$  and  $\phi(r)$  do not depend on  $m$ . This means that a change in  $m$ , namely

$$m \Rightarrow m'$$

must leave eq.(5.1) invariant, which implies

$$\frac{T_0}{m} = \text{invariant} \quad , \quad m^4 \exp \left[ \frac{\mu(r)}{T_0} \right] = \text{invariant}.$$

That is,

$$T_0(m') = \frac{m'}{m} T_0(m) \quad , \quad \mu(m', r) = \frac{m'}{m} \left[ \mu(m, r) + 4 T_0(m) \ln \left( \frac{m}{m'} \right) \right]. \quad (5.3)$$

A change in the WDM particle mass  $m$  implies that the temperature  $T_0$  and the chemical potential  $\mu(r)$  transform as given by eq.(5.3). These transformations leave the Boltzmann gas equations (5.1)-(5.2) invariant.

Under changes of  $m$  the dimensionless variables  $\xi$  and  $\nu(\xi)$  transform as

$$m \Rightarrow m' \quad , \quad \xi' = \xi \left( \frac{m'}{m} \right)^2 \quad , \quad \nu(\xi', m') = \nu(\xi, m) + 4 \ln \left( \frac{m}{m'} \right). \quad (5.4)$$

We see that all the diluted regime relations eqs.(2.37)-(2.47) are invariant under the change  $m \Rightarrow m'$  implemented through eqs.(5.3)-(5.4).

Indeed, this invariance is restricted to the diluted regime ( $\hat{M}_h \gtrsim 10^6 M_\odot$ ).

For galaxy masses  $\hat{M}_h < 10^5 M_\odot$ , namely in the **quantum regime of compact dwarf galaxies**, all physical quantities **do depend** on the DM particle mass  $m$  as explicitly displayed in eqs.(2.17)-(2.35). It is precisely this dependence on  $m$  that leads to the lower bound  $m > 1.91$  keV from the minimum observed galaxy mass [8]. Moreover, for  $m > 2$  keV, an overabundance of small structures appear as solution of the Thomas-Fermi equations, which do not have observed counterpart. Therefore,  $m$  between 2 keV and 3 keV is singled out as the most plausible value [8].

In summary, we see the power of the WDM Thomas-Fermi approach to describe the structure and the physical state of galaxies in a clear way and in very good agreement with observations.

[1] Anderhalden D. et al. arXiv:1212.2967, JCAP, 03, 014 (2013).

[2] V. Avila-Reese et al., Ap J, 559, 516 (2001).

[3] J. Binney and S. Tremaine, 'Galactic Dynamics', 2nd. edition, Princeton Univ. Press, 2008.

- [4] P. Colín, O. Valenzuela, V. Avila-Reese, *Ap J*, 542, 622 (2000).
- [5] P. Colín, O. Valenzuela, V. Avila-Reese, *Ap J*, 673, 203 (2008).
- [6] *Cosmic Frontier*, H. J. de Vega, N. G. Sanchez arXiv:1304.0759.
- [7] C. Destri, H. J. de Vega, N. G. Sanchez, *New Astronomy* **22**, 39 (2013).
- [8] C. Destri, H. J. de Vega, N. G. Sanchez, *Astrop. Phys.*, **46**, 14 (2013).
- [9] F. Munyaneza, P. L. Biermann, A & A, 458, L9 (2006). P. H. Chavanis, *Phys. Rev.* **E65**, 056123 (2002), P. H. Chavanis, *Int. J. Mod. Phys. B*20, 3113 (2006).
- [10] H. J. de Vega, N. G. Sánchez, *Nuclear Physics B* **625**, 409 and 460 (2002).
- [11] H. J. de Vega, N. G. Sánchez, *Mon. Not. R. Astron. Soc.* **404**, 885 (2010).
- [12] H. J. de Vega, P. Salucci, N. G. Sanchez, *New Astronomy* **17**, 653 (2012).
- [13] H. J. de Vega, P. Salucci, N. G. Sanchez, arXiv:1309.2290.
- [14] F. Donato et al., *MNRAS* **397**, 1169 (2009).
- [15] L. Gao and T. Theuns, *Science*, 317, 1527 (2007).
- [16] Highlights and Conclusions of the Chalonge 16th Paris Cosmology Colloquium 2012, arXiv:1307.1847.
- [17] Highlights and Conclusions of the Chalonge Meudon Workshop 2012 arXiv:1305.7452.
- [18] J Kormendy, K C Freeman, *IAU Symposium*, Sydney, 220, 377 (2004), arXiv:astro-ph/0407321.
- [19] L D Landau and E M Lifshits, *Statistical Mechanics*, Elsevier, Oxford, 1980.
- [20] M. R. Lovell et al., *MNRAS*, 420, 2318 (2012).
- [21] M. R. Lovell et al. arXiv:1308.1399.
- [22] A. Macciò, S. Paduroiu, D. Anderhalden, A. Schneider, B. Moore, *MNRAS* 424, 1105 (2012).
- [23] A. W. McConnachie, *AJ*, 144, 4 (2012).
- [24] N. Menci, F. Fiore, A. Lamastra, *ApJ*, 766, 110 (2013).
- [25] A. M. Nierenberg et al. arXiv:1302.3243, to appear in *ApJ*.
- [26] F. Pacucci et al. arXiv:1306.0009, to appear in *MNRAS Letters*.
- [27] E. Papastergis et al., *Ap J*, 739, 38 (2011).
- [28] P. Salucci et al. *MNRAS* **378**, 41 (2007).
- [29] G. Gilmore et al., *Ap J*, 663, 948 (2007).
- [30] M. Walker, J. Peñarrubia, *Ap. J.* 742, 20 (2011).
- [31] J. D. Simon, M. Geha, *Ap J*, 670, 313 (2007) and references therein. J. D. Simon et al., *Ap. J.* 733, 46 (2011) and references therein. J. Wolf et al., *MNRAS*, 406, 1220 (2010) and references therein. J. P. Brodie et al., *AJ*, 142, 199 (2011). G. D. Martinez et al., *Ap J*, 738, 55 (2011). B. Willman and J. Strader, *AJ*, 144, 76 (2012).
- [32] S. Shao et al. *MNRAS*, 430, 2346 (2013).
- [33] J. Sommer-Larsen, A. Dolgov, *Ap J*, 551, 608 (2001).
- [34] M. Spano et al., *MNRAS*, 383, 297 (2008).
- [35] A. V. Tikhonov et al., *MNRAS*, 399, 1611 (2009).
- [36] J. Viñas, E. Salvador-Solé, A. Manrique, *MNRAS* 424, L6 (2012).
- [37] C. R. Watson, Z. Li, N. Polley, *JCAP* 03, 018 (2012).
- [38] J. Zavala et al., *Ap J*, 700, 1779 (2009).
- [39] R. F. G. Wyse, G. Gilmore, *IAU Symposium*, Vol. 244, p. 44-52 (2007), arXiv:0708.1492. J. van Eymeren et al. *A & A* 505, 1-20 (2009). W. J. G. de Blok, *Advances in Astronomy*, vol. 2010, pp. 1-15, (2010), arXiv:0910.3538. P. Salucci, Ch. Frigerio Martins, arXiv:0902.1703, *EAS Publications Series*, 36, 2009, 133-140.